Editors' Suggestion

# Origin of Magic Angles in Twisted Bilayer Graphene

Grigory Tarnopolsky, Alex Jura Kruchkov,* and Ashvin Vishwanath
*Department of Physics, Harvard University, Cambridge, Massachusetts 02138, USA*

(Received 24 November 2018; published 15 March 2019; corrected 16 May 2019)

Twisted bilayer graphene (TBG) was recently shown to host superconductivity when tuned to special "magic angles" at which isolated and relatively flat bands appear. However, until now the origin of the magic angles and their irregular pattern have remained a mystery. Here we report on a fundamental continuum model for TBG which features not just the vanishing of the Fermi velocity, but also the perfect flattening of the entire lowest band. When parametrized in terms of $\alpha \sim 1/\theta$, the magic angles recur with a remarkable periodicity of $\Delta\alpha \simeq 3/2$. We show analytically that the exactly flat band wave functions can be constructed from the doubly periodic functions composed of ratios of theta functions—reminiscent of quantum Hall wave functions on the torus. We further report on the unusual robustness of the experimentally relevant first magic angle, address its properties analytically, and discuss how lattice relaxation effects help justify our model parameters.

DOI: 10.1103/PhysRevLett.122.106405

*Introduction.*—The recent discovery of correlated insulation and seemingly unconventional superconductivity in twisted bilayer graphene (TBG) [1–3] has revived interest in TBG [4–28]. Importantly, these phenomena are observed in a narrow range of twist angles near 1.05°, i.e., the first *magic angle* where the isolated and relatively flat band appear near neutrality [29–33]. To date, the origin and recurrence of the magic angles is not clear, even whether it is a fundamental feature or an outcome of engineering material parameters. Below we show that the appearance of the exactly flat band is a fundamental feature, with a remarkable mathematical structure that is exposed in this Letter.

Two graphene sheets rotated ("twisted") by a small relative angle form a long-periodic moiré pattern. For small angles $\theta$, the distinction between commensurate and incommensurate structures can be ignored, giving the lowest branch of moiré periods as $L(\theta) = a_0/2\sin\theta/2$ ($a_0$ is graphene lattice constant). The electronic structure of small-angle TBGs was previously addressed by Bistritzer and MacDonald [29] who reported band flattening and introduced the concept of magic angles (see also Refs. [30–32,34] and [35–37]). Recently, several groups have used the continuum model and studied the role of topology of flat bands near the magic angles [4,6,13,19,21,38–41]. Currently, the nature of superconductivity in this system is still being debated; however it is clear that the flat bands emerging at the magic angles are key. However, despite recent advances, the origin of the magic angles and flat bands in TBG remains mysterious.

In this Letter, we consider a continuum model, which is parametrized by interlayer coupling parameters $w_{AA}$ and $w_{AB}$ for $AA$ and $AB$ bilayer stacking, respectively. Earlier studies [29,30,32,34] set $w_{AA} = w_{AB}$, which gives band flattening in the gapless model. In reality, for TBG at tiny twist angles the gap opens and also $w_{AA}/w_{AB}$ is suppressed due to lattice relaxation effects [21,38,42]. As an idealization, we consider a continuum model with $w_{AA} = 0$ that acquires a chiral symmetry (a unitary particle-hole symmetry). In this chirally symmetric continuum model we switch off $AA$ coupling completely but keep $AB$ and $BA$ finite, and to our surprise a number of physical phenomena reveal at the magic angles. Not only do the Fermi velocities of the moiré Dirac points vanish, the entire band becomes *perfectly* flat at the recurrent set of magic angles (see Fig. 1). The sequence of magic angles that we find reveals a remarkable asymptotic periodicity of $\Delta\alpha \simeq 3/2$ which is not present in the $w_{AA} = w_{AB}$ case (see Table I). Moreover, the band gap is maximized at the same set of angles. We conclude that because of its remarkable properties, this is the fundamental model that concisely captures the magic angle phenomena. The flatness at magic angles is not just a matter of engineering material properties, but has deep hidden analytical connections to quantum Hall wave functions [43] and index theorems which we reveal.

*Continuum model for twisted bilayer graphene.*—The continuum model describing a single valley of TBG considers two layers of graphene described by Dirac fields at $K$, $K'$ points of the moiré (mini) Brillouin zone (mBZ), each rotated by an angle $\pm\theta/2$, and coupled through moiré potential $T(\mathbf{r})$ [4,13,29,34]:

$$H = \begin{pmatrix} -iv_0\boldsymbol{\sigma}_{\theta/2}\boldsymbol{\nabla} & T(\mathbf{r}) \\ T^\dagger(\mathbf{r}) & -iv_0\boldsymbol{\sigma}_{-\theta/2}\boldsymbol{\nabla} \end{pmatrix}, \tag{1}$$

where $\boldsymbol{\sigma}_{\theta/2} = e^{-(i\theta/4)\sigma_z}(\sigma_x,\sigma_y)e^{(i\theta/4)\sigma_z}$, $\nabla = (\partial_x,\partial_y)$ and $T(\mathbf{r}) = \sum_{n=1}^{3} T_n e^{-i\mathbf{q}_n\mathbf{r}}$, where $\mathbf{q}_1 = k_\theta(0,-1)$, $\mathbf{q}_{2,3} = k_\theta(\pm\sqrt{3}/2, 1/2)$ are responsible for the moiré pattern structure with the modulation $k_\theta = 2k_D\sin(\theta/2)$; here

 

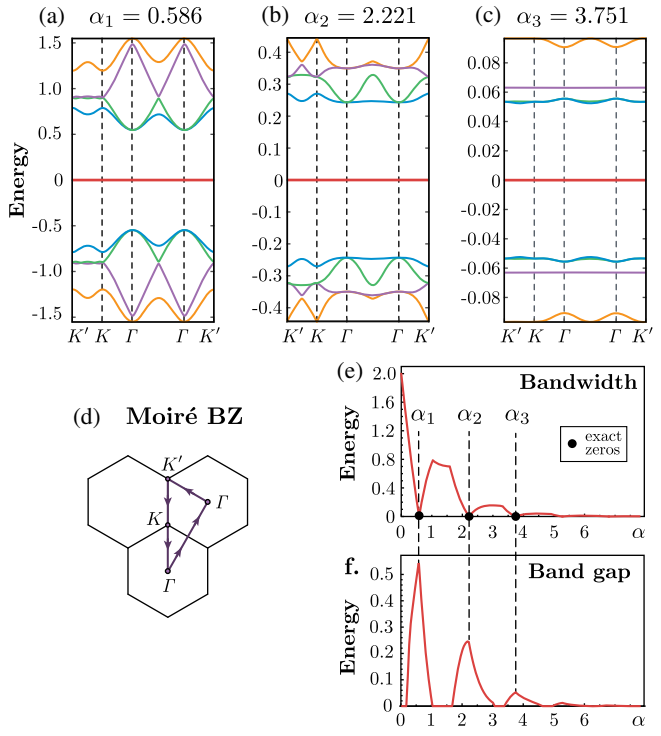


FIG. 1. Absolutely flat bands in continuum TBG Hamiltonian (1) with $w_{AA} = 0$ appear at exact magic angles parameters $\alpha = 0.586,\ 2.221,\ 3.751$, etc. (Here $\alpha = w_{AB}/2v_0k_D \sin\theta/2$ and energy in units $w_{AB}/\alpha$). On subfigures (a)–(c), the band is numerically flat to an accuracy $10^{-16}$. (d) Moiré Brillouin zone. (e)–(f) The band width drops exactly to zero at the set of magic angles. At the same points, we observe maxima of the band gaps.

$k_D = 4\pi/(3a_0)$ is the Dirac momentum. The Hamiltonian (1) acts on the spinor $\Phi(\mathbf{r}) = (\psi_1, \chi_1, \psi_2, \chi_2)^T$ and the indices 1,2 represent the graphene layer. The symmetries of TBGs allow interlayer coupling of the form

$$T_{n+1} = w_{AA}\sigma_0 + w_{AB}(\sigma_x \cos n\phi + \sigma_y \sin n\phi), \quad \phi = 2\pi/3.$$

Because of energetically preferred Bernal stacking at zero twist, the relative strength $w_{AA}/w_{AB}$ is suppressed at tiny angles [38]; thus the fundamental features of the TBGs can be expected when only $w_{AB}$ is present.

*Chirally symmetric continuum model.*—In this Letter, we study a pristine model of Eq. (1) with $w_{AA} = 0$. First, one can eliminate the twists in kinetic terms, $\boldsymbol{\sigma}_{\pm\theta/2} \to \boldsymbol{\sigma}$ by rotating the spinors. Then, by reshuffling the spinor to $\Phi(\mathbf{r}) = (\psi_1, \psi_2, \chi_1, \chi_2)^{\mathrm{T}}$, the chirally symmetric model reads

$$\mathcal{H} = \begin{pmatrix} 0 & \mathcal{D}^*(-\mathbf{r}) \\ \mathcal{D}(\mathbf{r}) & 0 \end{pmatrix}, \quad \mathcal{D}(\mathbf{r}) = \begin{pmatrix} -2i\bar{\partial} & \alpha U(\mathbf{r}) \\ \alpha U(-\mathbf{r}) & -2i\bar{\partial} \end{pmatrix}, \tag{2}$$

where $\bar{\partial} = \frac{1}{2}(\partial_x + i\partial_y)$ and $U(\mathbf{r}) = e^{-i\mathbf{q}_1\mathbf{r}} + e^{i\phi}e^{-i\mathbf{q}_2\mathbf{r}} + e^{-i\phi}e^{-i\mathbf{q}_3\mathbf{r}}$. Note that Hamiltonian $\mathcal{H}$ has only one dimensionless parameter $\alpha = w_{AB}/(v_0k_\theta)$ which fully controls the physics of the system [44].

Our chirally symmetric Hamiltonian (2) has several pronounced properties rooting towards the fundamental nature of the magic angles in TBGs. First, due to particle-hole symmetry, $\{\mathcal{H}, \sigma_z \otimes 1\} = 0$, the band structure of this Hamiltonian is symmetric with respect to $\varepsilon = 0$. Second, the entire lowest band becomes absolutely flat (that is, with zero bandwidth in the entire mBZ) at the recurrent values of $\alpha$ corresponding to the magic angles $\theta$ of this model (see Fig. 1). Moreover, the band gaps are maximized for the magic $\alpha$ where the bandwidth is exactly zero. For example, the first magic angle of our model is given by $\alpha_1 \approx 0.586$, which corresponds to $\theta \approx 1.09°$ on taking $w_{AB} = 110$ meV and $2v_0k_D = 19.81$ eV. Finally, we report that the magic angles in our model follow a remarkable recurrence with period $\Delta\alpha \simeq 3/2$ (see Fig. 2) which saturates very fast. We note, however, in the continuum models with finite $AA$ coupling ($w_{AA} \neq 0$), this feature is smeared away and the pattern is lost for large $w_{AA}$. The fundamental features of the absolutely flat bands, the pronounced band gaps, and the very strong periodicity in magic angles of the chirally symmetric continuum model (2) indicate that this model captures the origin of the magic angles in the most precise way. Previously the magic angles were defined as twists for which the Fermi velocity vanishes in Dirac points. Instead, we redefine the notion of magic angles (at arbitrary $w_{AA}$) as twists where the bandwidth is minimized (useful for numerics at $w_{AA} \neq 0$). A striking result of this Letter is not just the vanishing of the Fermi velocity, but the flattening of the entire lowest band in the limit $w_{AA} \to 0$. Below we reveal the absolutely flat band solution in TBG is linked to flatness of the lowest Landau level in quantum Hall effect on torus [43].

*Absolutely flat bands.*—We start from an observation that the TBG model (2) always has two zero modes at points $K$ and $K'$ of the mBZ, for all $\alpha$. This is due to a symmetry feature $\mathcal{D}(R_\phi\mathbf{r}) = \omega\mathcal{D}(\mathbf{r})$ which holds for all $\alpha$, where $R_\phi$ denotes a counterclockwise rotation by $\phi = 2\pi/3$ and $\omega = e^{i\phi}$. It is possible to construct an operator $\mathcal{R} = u_\phi e^{\phi\mathbf{r}\times\partial_\mathbf{r}}$, with diagonal matrix $u_\phi = \mathrm{diag}(1, e^{-i\phi})$, which commutes with the Hamiltonian $[\mathcal{R}, \mathcal{H}(\mathbf{r})] = 0$. Therefore, each eigenfunction of Hamiltonian $\mathcal{H}$ can be uniquely labeled by $C_3$ rotation eigenvalue: 1, $\omega$, $\omega^*$. We now consider case $\alpha = 0$, for which Hamiltonian (2) has four zero modes: two from

TABLE I. Magic angles in models with $w_{\mathrm{AA}} = 0$ and $w_{\mathrm{AA}} = w_{\mathrm{AB}}$. Only the principal magic angles $\alpha_1$ coincide.

| | $\alpha_1$ | $\alpha_2$ | $\alpha_3$ | $\alpha_4$ | $\alpha_5$ |
|---|---|---|---|---|---|
| $w_{\mathrm{AA}} = 0$ (here) | 0.586 | 2.221 | 3.75 | 5.28 | 6.80 |
| $w_{\mathrm{AA}} = w_{\mathrm{AB}}$ ([29]) | 0.606 | 1.27 | 1.82 | 2.65 | 3.18 |

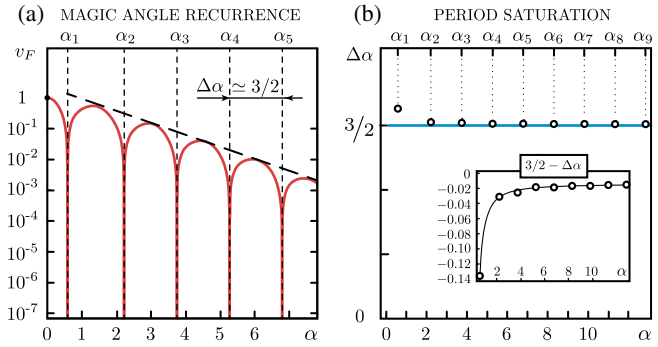


FIG. 2. Magic angle recurrence: (a) Fermi velocity at $K$, $K'$ as a function of magic angle parameter $\alpha$ (logarithmic scale). The sequence of the magic angles follows the asymptotic "3/2" rule: distance between adjacent $\alpha$'s is "quantized" with $\Delta\alpha \simeq 3/2$, which saturates very fast, see (b).

each Dirac points. Dirac points $K$ and $K'$ differ in their $C_3$ rotation eigenvalue: $\omega$, and $\omega^*$ see, e.g., Ref. [4]. Since $\mathcal{R}$ also commutes with the particle-hole transformation, $[\mathcal{R}, \sigma_z \otimes 1] = 0$, we can consider each zero mode of $K$ (or $K'$) individually. Turning on $\alpha > 0$ gradually, which preserves symmetry, each zero modes being unique must remain at zero energy.

Using the fact that there are always zero modes in some points of mBZ, we now explain the origin of the absolutely flat band in our model $(\mathcal{H}\Phi_{\mathbf{k}}(\mathbf{r}) = \varepsilon_0(\mathbf{k})\Phi_{\mathbf{k}}, \varepsilon_0(\mathbf{k}) = 0)$. The appearance of the perfectly flat band at the set of magic angles implies that the zero-energy equation [see Eq. (2)]

$$\mathcal{D}(\mathbf{r})\psi_{\mathbf{k}}(\mathbf{r}) = 0 \tag{3}$$

has solutions for arbitrary momenta $\mathbf{k}$ in the mBZ, and the two component wave function $\psi_{\mathbf{k}}(\mathbf{r})$ should obey the double-periodic moiré boundary conditions on translation vectors $\mathbf{a}_{1,2} = (4\pi/3k_\theta)[\pm(\sqrt{3}/2), \frac{1}{2}]$,

$$\psi_{\mathbf{k}}(\mathbf{r}+\mathbf{a}_{1,2}) = e^{i\mathbf{k}\mathbf{a}_{1,2}} U_\omega \psi_{\mathbf{k}}(\mathbf{r}), \quad U_\omega = \mathrm{diag}(1, \omega^*). \tag{4}$$

As explained above, Eq. (3) has always the zero-mode solution $\psi_K(\mathbf{r})$ at Dirac point $K$ with the property $\psi_K(\mathbf{r}+\mathbf{a}_{1,2}) = u_\phi \psi_K(\mathbf{r})$. The kinetic part of operator $\mathcal{D}(\mathbf{r})$ is completely antiholomorphic (that is, contains only $\bar\partial$ but no $\partial$). Thus one can multiply the zero mode solution $\psi_K(\mathbf{r})$ by any complex function $f(z)$ of single variable $z = x + iy$,

$$\psi_{\mathbf{k}}(\mathbf{r}) = f_{\mathbf{k}}(z)\psi_K(\mathbf{r}). \tag{5}$$

It is possible to find a function $f_{\mathbf{k}}(z)$ obeying moiré boundary conditions $f_{\mathbf{k}}(z + a_{1,2}) = e^{i\mathbf{k}\mathbf{a}_{1,2}} f_{\mathbf{k}}(z)$ with $a_{1,2} = (\mathbf{a}_{1,2})_x + i(\mathbf{a}_{1,2})_y$. Such a function $f_{\mathbf{k}}(z)$ must have a simple pole. We stress that in general such a construction (5) fails to work, as $\psi_{\mathbf{k}}(\mathbf{r})$ is unwillingly singular. The true "magic" happens exactly at the magic angles (see Fig. 3): the two-component spinor $\psi_K(\mathbf{r})$ drops to zero at the $BA$ stacking point $\psi_K(\mathbf{r}_0) = 0$, where $\mathbf{r}_0 = \frac{1}{3}(\mathbf{a}_1 - \mathbf{a}_2)$. Thus, we find the flat band solution

$$\psi_{\mathbf{k}}(\mathbf{r}) = \frac{\vartheta_{(\mathbf{k}\mathbf{a}_1/2\pi)-\frac{1}{6},\frac{1}{6}-(\mathbf{k}\mathbf{a}_2/2\pi)}(z/a_1|\omega)}{\vartheta_{-\frac{1}{6},\frac{1}{6}}(z/a_1|\omega)}\psi_K(\mathbf{r}), \tag{6}$$

where $\vartheta_{a,b}(z|\tau)$ is the theta function with rational characteristics $a$ and $b$ defined as [46]

$$\vartheta_{a,b}(z|\tau) = \sum_{n=-\infty}^{+\infty} e^{i\pi\tau(n+a)^2} e^{2\pi i(n+a)(z+b)}.$$

Under this construction, the zeros of $\psi_K(\mathbf{r})$ *exactly* cancel zeros of the theta function in the denominator. Using properties of the theta function [46], one can verify that solution (6) obeys boundary conditions (4). Therefore, exactly at the magic angles, where $\psi_K(\mathbf{r_0}) = 0$, the wave functions (6) satisfy the zero-mode Eq. (3) for all momenta $\mathbf{k}$. Thus we showed that there is a perfectly flat band $\varepsilon_0(\mathbf{k}) \equiv 0$ in entire mBz. The wave function (6) is reminiscent of lowest Landau level wave functions on the torus [43], familiar from the quantum Hall effect. This connection indicates that the flatness in TBG is not just a lucky choice of material parameters, but a fundamental feature of the TBG physics.

*Zero mode equation and Fermi velocity.*—We now show that zero Fermi velocity is also connected to the zeros of wave functions $\psi_K(\mathbf{r})$ appearing at the magic angles. The zero-mode equation at $K$ point reads $\mathcal{D}(\mathbf{r})\psi_K(\mathbf{r}) = 0$ with spinor $\psi_K(\mathbf{r}) = (\psi_{K,1}, \psi_{K,2})^{\mathrm{T}}$. The renormalized Fermi velocity can be found through first-order perturbation theory

$$v_F(\alpha) = \left| \partial_{\mathbf{k}} \frac{\langle \Phi_K | V_{\mathbf{k}} | \Phi_K \rangle}{\langle \Phi_K | \Phi_K \rangle} \right|_{\mathbf{k}=0}, \qquad V_{\mathbf{k}} = \begin{pmatrix} 0 & \bar{k} \\ k & 0 \end{pmatrix},$$

where $k$, $\bar{k} = (k_x \pm i k_y)\sigma_0$ and $\Phi_K(\mathbf{r}) = (\psi_K, \chi_K)^{\mathrm{T}}$. This implies

$$v_F(\alpha) = \frac{|\langle \psi_K^*(-\mathbf{r}) | \psi_K(\mathbf{r}) \rangle|}{\langle \psi_K | \psi_K \rangle}. \tag{7}$$

Because of the rotational symmetry of $\mathcal{D}(\mathbf{r})$ discussed above, one concludes that if $\psi_K(\mathbf{r})$ is a solution to the equation $\mathcal{D}(\mathbf{r})\psi_K(\mathbf{r}) = 0$, then $\psi_K(R_\phi \mathbf{r})$ is also a solution. This, in particular, implies at arbitrary $\alpha$ relations $\psi_{K,1}(R_\phi \mathbf{r} \pm \mathbf{r}_0) = \psi_{K,1}(\mathbf{r} \pm \mathbf{r}_0)$ and $\psi_{K,2}(R_\phi \mathbf{r} \pm \mathbf{r}_0) = e^{\pm i\phi}\psi_{K,2}(\mathbf{r} \pm \mathbf{r}_0)$. The second relation means that $\psi_{K,2}(\mathbf{r})$ always vanishes at $\mathbf{r} = \pm\mathbf{r}_0$ (i.e., for all $\alpha$); however $\psi_{K,1}(\mathbf{r})$ is in general nonzero. To relate appearance of zeros in $\psi_K(\mathbf{r})$ to zeros of the renormalized Fermi velocity, we notice that the Fermi velocity is proportional to an integral of motion of the operator $\mathcal{D}(\mathbf{r})$,

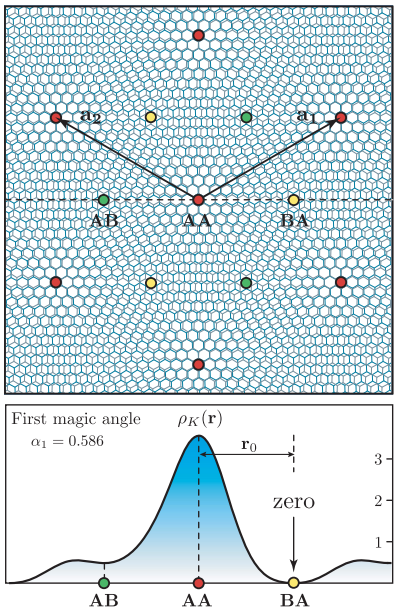


FIG. 3. (top) Schematic moiré pattern with regions referred to in the text marked. (bottom) Wave function density $\rho_K(\mathbf{r}) = \psi_K^\dagger \psi_K$ in real space for a single zero mode at the Dirac point $K$: $\rho_K(\mathbf{r})$ is localized on $AA$ stacking and (exactly at the magic angles) has zeros on $BA$ stacking.

$$v(\alpha) = \psi_{K,1}(\mathbf{r})\psi_{K,1}(-\mathbf{r}) + \psi_{K,2}(\mathbf{r})\psi_{K,2}(-\mathbf{r}), \quad (8)$$

where $v(\alpha)$ does not depend on coordinates and from Eq. (7) we see that $v_F(\alpha) \sim v(\alpha)$. Thus, because $\psi_{K,2}(\pm\mathbf{r}_0) = 0$, we find $v_F(\alpha) \sim \psi_{K,1}(\mathbf{r}_0)\psi_{K,1}(-\mathbf{r}_0)$. Therefore the vanishing of the Fermi velocity $v_F(\alpha) = 0$ means that either $\psi_{K,1}(\mathbf{r}_0)$ or $\psi_{K,1}(-\mathbf{r}_0)$ is zero and vice versa. This is the same argument that gave rise to appearance of the absolutely flat bands as was shown previously. Thus $v_F(\alpha) = 0$ implies the existence of the absolutely flat band with wave function Eq. (6). The appearance of zeros of the Fermi velocity $v_F(\alpha)$, and thus the appearance of flat bands, is not surprising, since $v_F(\alpha)$ is just a real function of a single parameter $\alpha$. By tuning this parameter, $v_F(\alpha)$ crosses zero at some value(s) of $\alpha$. To trace the appearance of the principal magic angle with $\alpha_1 \approx 0.586$ we use perturbation theory in $\alpha$, and compare the two definitions of magic angles.

*Principal magic angle.*—We start from the previous definition of magic angles [29] as twist angles at which the Fermi velocity vanishes. One can analyze the zero mode equation at Dirac point $K$ by using perturbation theory in magic angle parameter $\alpha < 1$, so spinor $\psi_K(\mathbf{r})$ has form

$$\psi_K(\mathbf{r}) = \begin{pmatrix} \psi_{K,1} \\ \psi_{K,2} \end{pmatrix} = \begin{pmatrix} 1 + \alpha^2 u_2 + \alpha^4 u_4 + \ldots \\ \alpha u_1 + \alpha^3 u_3 + \ldots \end{pmatrix}.$$

In general, one can find $u_n(\mathbf{r})$ step by step up to an arbitrary order in $\alpha$. Up to the eighth order we have

$$v_F(\alpha) = \frac{1 - 3\alpha^2 + \alpha^4 - \frac{111\alpha^6}{49} + \frac{143\alpha^8}{294} + \ldots}{1 + 3\alpha^2 + 2\alpha^4 + \frac{6\alpha^6}{7} + \frac{107\alpha^8}{98} + \ldots}. \quad (9)$$

Setting $v_F(\alpha) = 0$, this expression gives the first magic angle $\alpha_1 \approx 0.587$, which is very close to the value $\alpha_1 = 0.586$ obtained numerically. Therefore the perturbation theory for small $\alpha$ quantitively explains the appearance of $\alpha_1$ and hints to the appearance of the next magic at $\alpha \sim 2$. Note also that up to $\alpha^2$, $v_F \approx (1 - 3\alpha^2)/(1 + 6\alpha^2)$, —similar to what was reported in a model with $w_{AA} = w_{AB}$ [29]. Thus, due to the robustness of the first magic angle (see Fig. 4), $\alpha_1 \approx (1/\sqrt{3})$ is valid both for $w_{AA} = 0$ and $w_{AA} = w_{AB}$.

Alternatively, the appearance of the first magic angle could be traced through the new definition as the angle at which the bandwidth is minimized. In our system, the bandwidth of the flattened bands is determined by doubled energy at the center of the mBZ zone ($\Gamma$ is $\mathbf{k} = \mathbf{q}_1$ in our notations). The symmetries of the Hamiltonian (2) imply that $\chi_\Gamma(\mathbf{r}) = \lambda_\alpha \sigma_x \psi_\Gamma(\mathbf{r})$, where $\lambda_\alpha = \pm 1$, and one can also obtain that $\psi_{\Gamma,2}(\mathbf{r}) = i\mu_\alpha \psi_{\Gamma,1}(-\mathbf{r})$, where $\mu_\alpha = \pm 1$. The spectrum at the $\Gamma$ point is characterized by the equations $2\bar{\partial}\psi_{\Gamma,1} \mp \alpha U(\mathbf{r})\psi_{\Gamma,1}(-\mathbf{r}) = \varepsilon_\Gamma \psi_{\Gamma,1}(-x, y)$, where "−" captures all odd magic angles and "+" all even. Perturbatively one has

$$\varepsilon_\Gamma = 1 - 2\alpha + \frac{\alpha^2}{3} + \frac{2\alpha^3}{9} + \frac{5\alpha^4}{54} + \ldots \quad (10)$$

Demanding the zero bandwidth at the first magic angle, we get $\alpha_1 \approx 0.585$, which is very close to the numerical result $\alpha_1 = 0.586$. Thus both in terms of Fermi velocity at Dirac points or the bandwidth minimization, the principal magic angle can be calculated very precisely and its value is the same as reported in experiments.

*Tuning the AA coupling strength.*—We have proposed a realistic symmetric model with perfectly flat bands, yet other models with flattened bands at finite $w_{AA}/w_{AB} < 1$ can be considered as perturbations around the exactly flat band model. To explore this, we now turn on $AA$ coupling back [$w_{AA} \neq 0$ in $T(\mathbf{r})$], and still neglect relative rotations in the kinetic terms $\boldsymbol{\sigma}_{\pm\theta/2} \to \boldsymbol{\sigma}$. We present the numerical dependence for the gap between the lowest band and the next excited band at the first two magic angles as a function of $w_{AA}/w_{AB}$ (see Fig. 4). Tuning on $w_{AA}$ smears out such fundamental features as zero bandwidth coexisting with maximized band gap, and the overall pattern of the magic angles, making higher-order magic angles badly defined. Importantly, the first magic angle is very robust against tuning $w_{AA}/w_{AB}$ continuously towards 1, until the band gap closes. This is a general feature of all magic angles which are robust until the first gap closing.

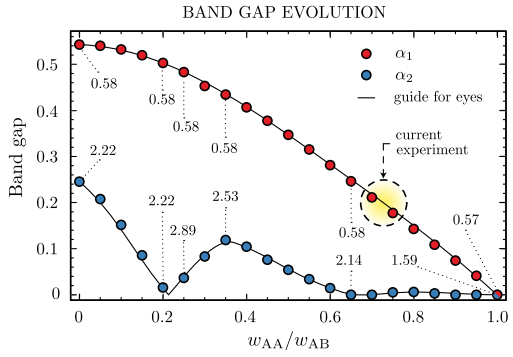


FIG. 4. Band gap evolution in the flow from our chirally symmetric model ($w_{AA} = 0$) to the gapless model ($w_{AA} = w_{AB}$). The first magic angle (red dots with local values of $\alpha_1$) remains robustly defined, while both the second magic angle and the corresponding band gap (blue dots with local $\alpha_2$) experience oscillations and discontinuities.

Experimentally, due to the lattice relaxation effects we have at first magic angle $w_{AA}/w_{AB} \simeq 0.7$–$0.8$ which promotes the gap [21,38,42] (see positioning in Fig. 4). Taking into account the finite gap $\sim$30 meV observed experimentally [1,2], our chirally symmetric model is qualitatively closer to real life than the gapless $w_{AA}/w_{AB} = 1$ model. We also propose the second magic angle to occur around $\alpha_2 \approx 2$, which converts to $\theta_2 \approx 0.22° - 0.29°$, depending on the precise value of $w_{AA}(\theta)/w_{AB}(\theta)$, and $\theta_2$ robust in the range $w_{AA}/w_{AB} < 0.2$. It would be interesting to pursue the second magic angle in experiments.

In conclusion, we introduced a variant of the continuum model used to describe TBG, and show that the notion of magic angles acquires a remarkably robust character visible in several properties including the perfect flatness of the bands at neutrality. We showed that the emergence of the flat bands in TBGs is related to the flatness of the lowest Landau level in quantum Hall effect on torus. Given that the model has flat bands, the appearance of the principal magic angle can be precisely traced with perturbation theory in $\alpha$. A deeper explanation of the periodic pattern of higher magic angles would be of great interest to explore in the future. The chiral model captures the nature of the flatness phenomena and thus the source of magic angles in a minimal way, and points to a rich underlying mathematical structure, further investigations of which is left to future work.

We thank Bertrand Halperin and Subir Sachdev for useful comments. A. V. would like to thank Adrian Po, Liujun Zou, T. Senthil, and YiZhuang You for several discussions on TBG. A. J. K. thanks Sabrina Pasterski for useful comments. G. T. was supported by the Multidisciplinary University Research Initiatives (MURI) Grant No. W911NF-14-1-0003 from ARO and by DOE Grant No. de-sc0007870. A. J. K. was supported by the Swiss National Science Foundation (SNSF), Grant "Emergent Topological Electronics" P2ELP2_175278. A. V. was supported by the Simons Investigator Award and by NSF-DMR 1411343.

*akruchkov@g.harvard.edu

[1] Y. Cao, V. Fatemi, S. Fang, K. Watanabe, T. Taniguchi, E. Kaxiras, and P. Jarillo-Herrero, Unconventional superconductivity in magic-angle graphene superlattices, Nature (London) **556**, 43 (2018).

[2] Y. Cao, V. Fatemi, A. Demir, S. Fang, S. L. Tomarken, J. Y. Luo, J. D. Sanchez-Yamagishi, K. Watanabe, T. Taniguchi, E. Kaxiras, R. C. Ashoori, and P. Jarillo-Herrero, Correlated insulator behaviour at half-filling in magic angle graphene superlattices, Nature (London) **556**, 80 (2018).

[3] M. Yankowitz, S. Chen, H. Polshyn, K. Watanabe, T. Taniguchi, D. Graf, A. F. Young, and C. R. Dean, Tuning superconductivity in twisted bilayer graphene, Science **363**, eaav1910 (2019).

[4] H. C. Po, L. Zou, A. Vishwanath, and T. Senthil, Origin of Mott Insulating Behavior and Superconductivity in Twisted Bilayer Graphene, Phys. Rev. X **8**, 031089 (2018).

[5] A. Thomson, S. Chatterjee, S. Sachdev, and M. S. Scheurer, Triangular antiferromagnetism on the honeycomb lattice of twisted bilayer graphene, Phys. Rev. B **98**, 075109 (2018).

[6] L. Zou, H. C. Po, A. Vishwanath, and T. Senthil, Band structure of twisted bilayer graphene: Emergent symmetries, commensurate approximants, and wannier obstructions, Phys. Rev. B **98**, 085435 (2018).

[7] F. Guinea and N. R. Walet, Electrostatic effects and band distortions in twisted graphene bilayers, Proc. Natl. Acad. Sci. U.S.A. **115**, 13174 (2018).

[8] S. Carr, S. Fang, P. Jarillo-Herrero, and E. Kaxiras, Pressure dependence of the magic twist angle in graphene superlattices, Phys. Rev. B **98**, 085144 (2018).

[9] Y. Su and S.-Z. Lin, Pairing symmetry and spontaneous vortex-antivortex lattice in superconducting twisted-bilayer graphene: Bogoliubov-de gennes approach, Phys. Rev. B **98**, 195101 (2018).

[10] J. González and T. Stauber, Kohn-Luttinger Superconductivity in Twisted Bilayer Graphene, Phys. Rev. Lett. **122**, 026801 (2019).

[11] F. Wu, T. Lovorn, E. Tutuc, I. Martin, and A. H. MacDonald, Topological insulators in twisted transition metal dichalcogenide homobilayers, arXiv:1807.03311.

[12] D. K. Efimkin and A. H. MacDonald, Helical network model for twisted bilayer graphene, Phys. Rev. B **98**, 035404 (2018).

[13] N. F. Q. Yuan and L. Fu, Model for the metal-insulator transition in graphene superlattices and beyond, Phys. Rev. B **98**, 045103 (2018).

[14] C. Xu and L. Balents, Topological Superconductivity in Twisted Multilayer Graphene, Phys. Rev. Lett. **121**, 087001 (2018).

[15] M. Ochi, M. Koshino, and K. Kuroki, Possible correlated insulating states in magic-angle twisted bilayer graphene under strongly competing interactions, Phys. Rev. B **98**, 081102 (2018).

[16] F. Wu, A. H. MacDonald, and I. Martin, Theory of Phonon-Mediated Superconductivity in Twisted Bilayer Graphene, Phys. Rev. Lett. **121**, 257001 (2018).
[17] Y.-h. Zhang, D. Mao, Y. Cao, P. Jarillo-Herrero, and T. Senthil, Nearly flat Chern bands in moiré superlattices, Phys. Rev. B **99**, 075127 (2019).
[18] X.-c. Wu, K. A. Pawlak, C.-m. Jian, and C. Xu, Emergent Superconductivity in the weak Mott insulator phase of bilayer graphene Moiré superlattice, arXiv:1805.06906.
[19] J. Kang and O. Vafek, Symmetry, Maximally Localized Wannier States, and a Low-Energy Model for Twisted Bilayer Graphene Narrow Bands, Phys. Rev. X **8**, 031088 (2018).
[20] J. M. Pizarro, M. J. Calderón, and E. Bascones, The nature of correlations in the insulating states of twisted bilayer graphene, arXiv:1805.07303.
[21] M. Koshino, N. F. Q. Yuan, T. Koretsune, M. Ochi, K. Kuroki, and L. Fu, Maximally Localized Wannier Orbitals and the Extended Hubbard Model for Twisted Bilayer Graphene, Phys. Rev. X **8**, 031087 (2018).
[22] D. M. Kennes, J. Lischner, and C. Karrasch, Strong correlations and $d+id$ superconductivity in twisted bilayer graphene, Phys. Rev. B **98**, 241407 (2018).
[23] H. Isobe, N. F. Q. Yuan, and L. Fu, Superconductivity and Charge Density Wave in Twisted Bilayer Graphene, Phys. Rev. X **8**, 041041 (2018).
[24] L. Rademaker and P. Mellado, Charge-transfer insulation in twisted bilayer graphene, Phys. Rev. B **98**, 235158 (2018).
[25] J.-B. Qiao and L. He, Heterostrain engineering on twisted graphene bilayer around the first magic angle, Phys. Rev. B **98**, 235402 (2018).
[26] T.-F. Chung, Y. Xu, and Y. P. Chen, Transport measurements in twisted bilayer graphene: Electron-phonon coupling and landau level crossing, Phys. Rev. B **98**, 035425 (2018).
[27] M. Fidrysiak, M. Zegrodnik, and J. Spałek, Unconventional topological superconductivity and phase diagram for an effective two-orbital model as applied to twisted bilayer graphene, Phys. Rev. B **98**, 085436 (2018).
[28] T. J. Peltonen, R. Ojajärvi, and T. T. Heikkilä, Mean-field theory for superconductivity in twisted bilayer graphene, Phys. Rev. B **98**, 220504 (2018).
[29] R. Bistritzer and A. H. MacDonald, Moire bands in twisted double-layer graphene, Proc. Natl. Acad. Sci. U.S.A. **108**, 12233 (2011).
[30] R. Bistritzer and A. H. MacDonald, Moiré butterflies in twisted bilayer graphene, Phys. Rev. B **84**, 035440 (2011).
[31] J. M. B. Lopes dos Santos, N. M. R. Peres, and A. H. Castro Neto, Continuum model of the twisted graphene bilayer, Phys. Rev. B **86**, 155449 (2012).
[32] S. Shallcross, S. Sharma, E. Kandelaki, and O. A. Pankratov, Electronic structure of turbostratic graphene, **81**, 165105 (2010).
[33] A. Luican, G. Li, A. Reina, J. Kong, R. R. Nair, K. S. Novoselov, A. K. Geim, and E. Y. Andrei, Single-Layer Behavior and Its Breakdown in Twisted Graphene Layers, Phys. Rev. Lett. **106**, 126802 (2011).
[34] J. M. B. Lopes dos Santos, N. M. R. Peres, and A. H. Castro Neto, Graphene Bilayer with a Twist: Electronic Structure, Phys. Rev. Lett. **99**, 256802 (2007).
[35] G. Li, A. Luican, J. M. B. Lopes dos Santos, A. H. Castro Neto, A. Reina, J. Kong, and E. Y. Andrei, Observation of Van Hove singularities in twisted graphene layers, Nat. Phys. **6**, 109 (2010).
[36] G. Trambly de Laissardiere, D. Mayou, and L. Magaud, Localization of dirac electrons in rotated graphene bilayers, Nano Lett. **10**, 804 (2010).
[37] J. M. B. Lopes dos Santos, N. M. R. Peres, and A. H. Castro Neto, Continuum model of the twisted graphene bilayer, Phys. Rev. B **86**, 155449 (2012).
[38] S. Carr, S. Fang, Z. Zhu, and E. Kaxiras, Minimal model for low-energy electronic states of twisted bilayer graphene, arXiv:1901.03420.
[39] Z. Song, Z. Wang, W. Shi, G. Li, C. Fang, and B. A. Bernevig, All magic angles are stable topological, arXiv:1807.10676.
[40] K. Hejazi, C. Liu, H. Shapourian, X. Chen, and L. Balents, Multiple topological transitions in twisted bilayer graphene near the first magic angle, Phys. Rev. B **99**, 035111 (2019).
[41] H. C. Po, L. Zou, T. Senthil, and A. Vishwanath, Faithful tight-binding models and fragile topology of magic-angle bilayer graphene, arXiv:1808.02482.
[42] N. N. T. Nam and M. Koshino, Lattice relaxation and energy band modulation in twisted bilayer graphene, Phys. Rev. B **96**, 075311 (2017).
[43] F. D. M. Haldane and E. H. Rezayi, Periodic Laughlin-Jastrow wave functions for the fractional quantized Hall effect, Phys. Rev. B **31**, 2529 (1985).
[44] A similar idea of switching off $w_{AA}$ was used in Ref. [45]. It was argued there that Hamiltonian (2) viewed as for Dirac fermions propagating in a background $SU(2)$ non-Abelian gauge field $\mathbf{A}$.
[45] P. San-Jose, J. González, and F. Guinea, Non-Abelian Gauge Potentials in Graphene Bilayers, Phys. Rev. Lett. **108**, 216802 (2012).
[46] D. Mumford, *Tata Lectures on Theta I*, Progress in Mathematics (1983), Vol. 28, pp. XIII, 240.

*Correction:* The author contribution statement has been removed at the request of the authors.